A Chameleon AIEgen with Quintuple yet Controllable Thermal/Photo Switch for Advanced Information Encryption

Xinyuan He,[1] Baochuan Hu,[2] Xin Wang,[3] Xing Feng,[4] Xinyuan Wang,[1] Jianwei Sun,[1] Jacky W. Y. Lam,[1,*] Lianrui Hu,[2,*] and Ben Zhong Tang[1,5,6,*]

[1] Department of Chemistry, and the Hong Kong Branch of Chinese National Engineering Research Center for Tissue Restoration and Reconstruction, The Hong Kong University of Science and Technology, Clear Water Bay, Kowloon, Hong Kong, China

[2] Shanghai Key Laboratory of Green Chemistry and Chemical Processes, Shanghai Frontiers Science Center of Molecule Intelligent Syntheses, School of Chemistry and Molecular Engineering, East China Normal University, Shanghai, 200062, China

[3] College of Chemistry and Chemical Engineering, Inner Mongolia Key Laboratory of Fine Organic Synthesis, Institutes of Biomedical Sciences, Inner Mongolia University, Hohhot, 010021, China

[4] School of Material and Energy, Guangdong University of Technology, Guangzhou 510006, China

[5] Center for Aggregation-Induced Emission, South China University of Technology, Guangzhou, 510640, China

[6] School of Science and Engineering, Shenzhen Institute of Aggregate Science and Technology, The Chinese University of Hong Kong, Shenzhen, Guangdong, 518172, China

Abstract: Seeking new methods to realize multiple fluorescence changes in a single luminogenic system is of great importance for both chemistry and bionics research. However, due to the lack of proper strategies and functional motifs, novel chameleon luminogens with multiple switching and controllable models is still scarce. Herein, we reported a chromone-based aggregation-induced emission luminogen called *Z*-CDPM, which exhibited quintuple yet controllable thermochromic or photochromic behavior

under different conditions. Specifically, five different reactions were involved: (i) reversible *Z*/*E* isomerization and irreversible cyclization and elimination under thermal treatment, and (ii) photorearrangment of *Z*-CDPM and its thermal cyclized product DPXDC under UV irradiation. All single crystals were successfully obtained and these reactivities and reaction pathways were confirmed experimentally and theoretically. Accordingly, multiple-colored images and a quick response code with free fixing and erasing capabilities were developed for advanced information encryption. This work thus provides new sights into the design of multiresponsive luminogens and multifunctional systems.

Introduction

The coloration in animals has long fascinated scientists, especially for the dynamic coloration under external stimuli, which fulfill the multiple biological functions of animals desired to make a living.[1-4] For example, chameleons and cuttlefishes perform concealing coloration and blend with the environment timely, so as to avoid predators and prey[5,6]. Crested ibis chooses a shiny coloration for courtship during the mating season[7]. While the static adaptive coloration illustrates the smart coloration strategies of animals acquired for acclimatization, the advanced *in-situ* discoloration observed in few intelligent species further highlights the sensing and responding capabilities. Such excellent examples in nature thus make a serendipity coloration model system for the development of bionic intelligence technology.[8-13] Likewise, it also raises the interests of chemists to seek new methods to imitate such intriguing colorful patterns of animals and pursue ingenious functional biomimetic systems.

Stimuli-responsive luminogens refer to a series of smart materials that are frequently chosen for performing functional discoloration in artificial systems.[14,15] Although multicolor systems are currently implemented by utilizing a complex combination of monoresponsive luminogens,[16-19] scientists prefer a single multiresponsive luminogenic system for simplicity and repeatability. Besides, reaction-based responsive luminogens pave an easy way for conducting on-demand discoloration with good controllability. However, the reported multiresponsive luminogens often display a single, or a single type of chemical reactivity, which is not conducive to the diversification of control modes and ultimately limits the scope of applications.[20-26] Due to the advancement in synthetic organic chemistry, it is then anticipated to construct novel multifunctional luminogens by installing different types of functional units in one molecule. But one big challenge is how to maintain the activity of each functional unit and the corresponding spectral changes in such a hybrid molecule.[21] On the other hand, new kinds of functional motifs are highly desired to enrich the library of discoloration models. Also, photochromic behavior is indeed needed in view of the unique advantages of the noncontact coloration model and high spatiotemporal resolution in real applications.[27-33] Conceivably, if one molecule meets all these requirements and further possess "one active site for no less than two reactions" property to get rid of the tedious and time-consuming organic synthesis and purification processes, its limitless applications are expected.

In recent years, luminogens with aggregation-induced emission (AIE) has aroused the great interest of scientists, and meanwhile their intensified emission in the aggregate

state has validated its value for sensing and solid imaging.[34-40] Previously, we reported a chromone-based AIE luminogen called CMVMN which could undergo specific bioconjugation with primary amines to give red-shifted and enhanced fluorescence (Scheme S1 in the Electronic Supporting Information).[41] By introducing of an additional phenyl group, a arylvinyl-substituted chromone-based AIEgen called CPVCM was further developed, which could undergo both amination with primary amines and photoarrangement with self-reporting property.[42] A multi-colored quick response code and an all-round information encryption system based on CPVCM alone were realized, demonstrating its great potential for developing multifunctional systems. Notably, the reactions of CMVMN and CPVCM all occurred at the same position of the chromone ring, which demonstrated the possibility of utilizing chromone as a specific skeleton to develop functional molecules with "one active site for no less than two reactions" property. Therefore, we are wondering whether it is possible to obtain another arylvinyl-substituted chromone-based AIEgen that could undergo photoarrangement[42,43] and also other new chemical reactions at the same position of the chromone ring for further pursuing multiresponsive applications.

In this work, we designed and synthesized an simple AIEgen, namely (*Z*)-2-[3-(4-oxo-4H-chromen-3-yl)-1,2-diphenylallylidene]malononitrile and abbreviated as *Z*-CDPM (Scheme 1) that could undergo multiple yet controllable thermal and photo reactions. Under thermal treatment, *Z*-CDPM underwent *Z*/*E* isomerization to generate *E*-CDPM, whose thermal cyclization produced DPXDC. The thermal elimination of DPXDC finally gave DPXC. All *Z*-CDPM, *E*-CDPM and DPXDC displayed sensitive

photorearrangement processes under UV irradiation. The structure of all these six molecules were confirmed by the single crystal X-ray diffraction technique and their different photophysical properties in both solution and solid state were checked to validate their potential in performing functional discolorations. NMR titration and theoretical calculation were further conducted to study the mechanisms of these thermal and photoarrangement processes. By utilizing multiresponsive *Z*-CDPM and DPXDC, their dip-coated films were fabricated to realize colored images and dynamic quick response (QR) codes with free fixing and erasing capabilities. Thus, this work not only developed a novel small AIE skeleton with multiple yet controllable thermal and photo responses, but also opened a new venue for the development of multiresponsive luminogens and intelligent information encryption based on luminescent materials.

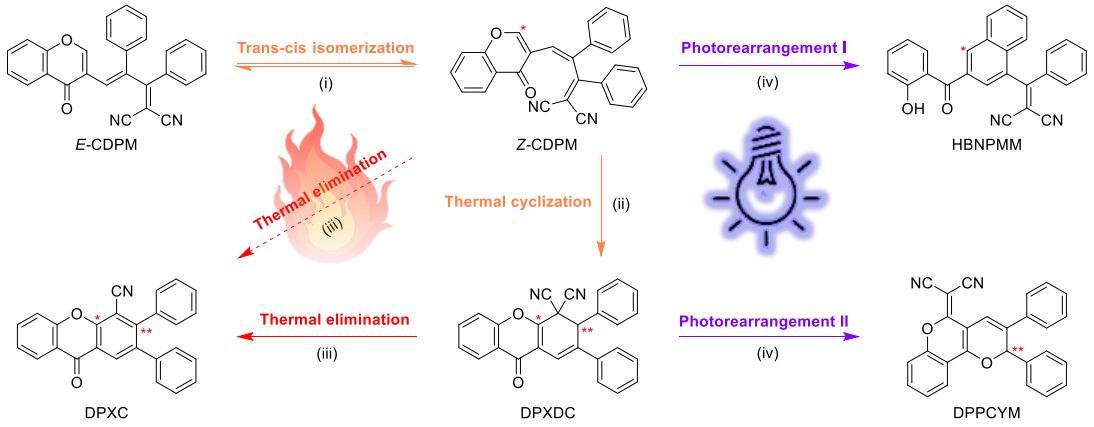

Scheme 1. Schematic illustration of the specific thermal and photo reactions of *Z*-CDPM under different conditions: (i) annealing at 145 °C in $C_2D_2Cl_4$ for 1 d; (ii) annealing at 145 °C in $C_2D_2Cl_4$ for 30 d; (iii) annealing at 145 °C in silica gel for 1 d; (iv) UV irradiation under a 365 nm UV lamp for 2 h. Notes: specific atoms of Z-CDPM and DPXDC involved in at least two reactions were highlighted with * and ** respectively.

Results and Discussion

Photophysical Properties. Photophysical properties and *Z*/*E* isomerization. *Z*-

CDPM and *E*-CDPM were both synthesized via a facile two-step process (Scheme S2). The intermediate and the final products were all characterized spectroscopically and satisfactory results corresponding to their molecular structures were acquired (Figure S1-S9). Also, single crystals were grown by a slow evaporation of a mixed solvent of dichloromethane (DCM) and petroleum ether (PE), and the corresponding single crystal X-ray diffraction data illustrated the twisted conformations of *Z*-CDPM and *E*-CDPM (Figure 1a and 1b and Table S1). In particular, two dihedral angles (ϕ(1,2,3,4) and ϕ(3,4,5,6)) observed in Z-CDPM (24.4°, 31.4°) were found to be much smaller than those of *E*-CDPM (43.7°, 59.5°), while another two dihedral angles (ϕ(3,4,7,8) and ϕ(8,7,9,10)) appeared similar and large for both two molecules. Such staggered conformations indicated the influence of steric effect on the molecular thermodynamic stability, and explained the simultaneous generation of two isomers (*Z*-CDPM and *E*-CDPM) in similar yields.

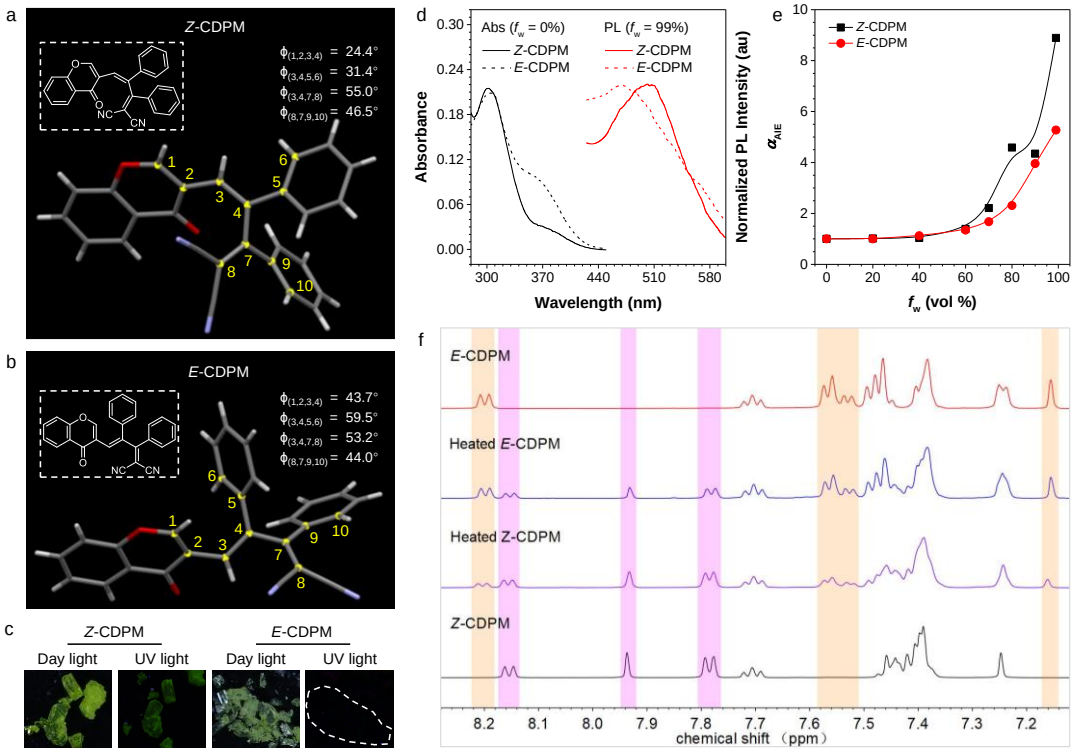

Figure 1. Single crystal structures of (a) *Z*-CDPM and (b) *E*-CDPM. Insets: chemical structures and dihedral angles in the crystal structures. (c) Photographs of crystals of *Z*-CDPM and *E*-CDPM. (d) Absorption and normalized photoluminescence (PL) spectra of *Z*-CDPM (solid line, 10 μM) and *E*-CDPM (dash line, 10 μM) in THF/water mixtures with different water fractions (f_w). (e) Plots of I/I_0 values versus the f_w of *Z*-CDPM (black, $\lambda_{ex/em}$ = 365/505 nm) and *E*-CDPM (red, $\lambda_{ex/em}$ = 350/480 nm), where I_0 = PL intensity in pure THF solution. (f) ^{1}H NMR spectra of as prepared *Z*-CDPM and *E*-CDPM before and after heating at 145 °C in $C_2D_2Cl_4$ for 1d. *Z*-CDPM was highlighted in purple, *E*-CDPM was highlighted in orange.

The photophysical properties of Z-CDPM and *E*-CDPM were then investigated. As shown in Figure 1c and Figure S10, the yellow crystals of Z-CDPM emitted dim greenish-yellow fluorescence, while the pale-yellow crystals of *E*-CDPM was found to be almost non-emissive. Their absorption and photoluminescence (PL) spectra in solution were also studied. Both Z-CDPM and *E*-CDPM showed an absorption peak in the visible region of 310 nm (Figure 1d), attributing to their poor conjugation.[41,42,44] *Z*-CDPM displayed also a shoulder absorption band at 365 nm in THF, and emitted weakly at 505 nm in THF/water mixture with a water fraction (f_w) of 99% (Figure S11). Due to the more twisted conformation of *E*-CDPM, its PL was observed at 480 nm instead. When a poor solvent of water was added to their THF solutions to promote the aggregate formation, gradually enhanced fluorescence was detected (Figure 1e and Figure S11), which confirmed their AIE properties.

To verify the conjecture of *Z*/*E* isomerization under thermal treatment, a deuterium reagent $C_2D_2Cl_4$ with high boiling point (b.p.) was chosen and utilized to prepare the

stock solutions for dynamic ^{1}H NMR analysis. Because of their different conjugation, *Z*-CDPM and *E*-CDPM showed obvious different ^{1}H NMR spectral patterns, and some characteristic peaks could be set as references for feasible investigation of the *Z*/*E* isomerization. As depicted in Figure 1f, the specific peaks of *E*-CDPM at δ 8.21-8.19, 7.58-7.52 and 7.16 were also found in the heated solution of *Z*-CDPM, and the ratio between the *Z*-isomer and the *E*-isomer was calculated to be 64:36 according to the related integral peak. Meanwhile, a similar phenomenon reappeared in the stock solution of *E*-CDPM and a ratio of 34:66 was obtained otherwise. Thus, a reversible yet controllable thermal *Z*/*E* isomerization was demonstrated for CDPM, as well as the thermodynamic stability of the two isomers. Based on the different emission properties of *Z*-CDPM and *E*-CDPM, it also provided new possibilities for the design of isomerization-based responsive luminogens.[45,46]

Thermal cyclization. When the heating process was prolonged, not only similar NMR peak intensities were detected in *Z*-CDPM and *E*-CDPM on day 5, but also several unexpected new peaks at δ 8.31-8.30 and 4.80 emerged (Figure 2a). Curiously, we conducted a quick test where *Z*-CDPM was dissolved in diphenyl ether (b.p. 258 ℃) and then heated it at 200 ℃ for 2 h (Scheme S3). Afterwards, a new molecule of DPXDC was isolated in a yield 87% and identified by single crystal X-ray diffraction (Figure 2b and Table S2). Satisfactory spectroscopical results corresponding to its molecular structure were obtained (Figure S12-S14), indicating a possible thermal cyclization reaction of *Z*-CDPM in solution.

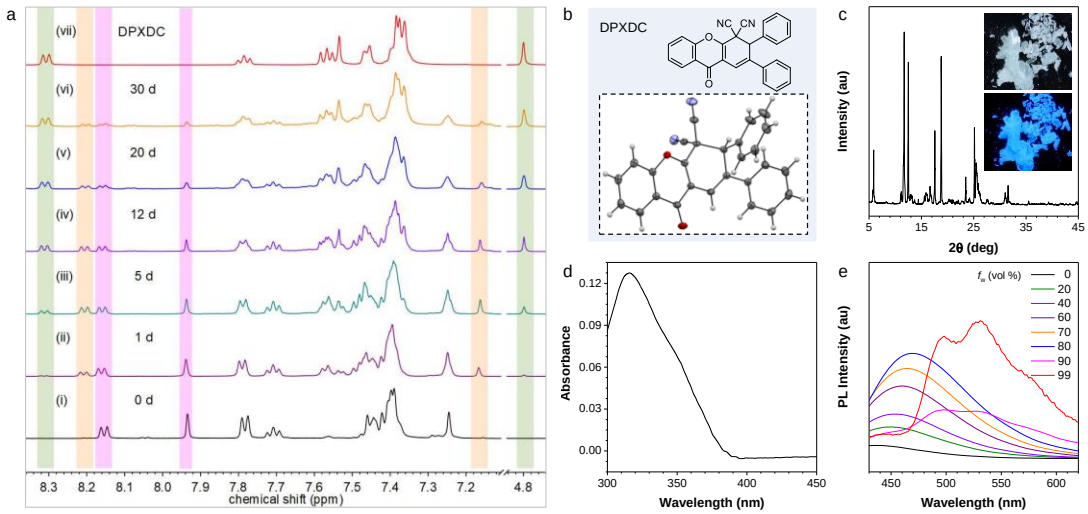

Figure 2. (a) ^{1}H NMR spectra of as prepared *Z*-CDPM before and after heating at 145 °C in $C_2D_2Cl_4$ for different time (1, 5, 12, 20, 30 d). *Z*-CDPM was highlighted in purple, *E*-CDPM was highlighted in orange, and DPXDC was highlighted in green. (b) Chemical and single crystal structures of DPXDC. (c) X-Ray diffraction (XRD) diffractograms of the crystal powder of DPXDC. Insets: photographs of crystals of DPXDC taken under day light (upper) and UV illumination (down). (d) Absorption spectra of DPXDC (10 μM) in THF. (e) PL spectra of DPXDC (10 μM) in THF/water mixtures. λ_{ex} = 365 nm.

The dynamic ^{1}H NMR analysis depicted an efficient but slow conversion of *Z*-CDPM to DPXDC in $C_2D_2Cl_4$ (Figure 2a). Specifically, the NMR peaks of DPXDC at δ 8.31-8.30 and 4.80 were gradually intensified during continuous heating, and eventually a ^{1}H NMR spectrum compared with that of DPXDC was obtained after 30 days of heating. Since the peaks in the aromatic range were well matched with those of *Z*/*E*-CDPM or DPXDC, a controllable thermal cyclization process and the solely generation of DPXDC were demonstrated. Even though a 30-day heating operation sounds meaningless in real applications, the high conversion rate of 87% obtained in the synthetic procedure provided a feasible method of increasing the temperature to

accelerate the thermal cyclization. To get a deeper insight, analysis by differential scanning calorimeter (DSC) in the range from 0 ℃ to 200 ℃ was conducted. The DSC curve of *Z*-CDPM exhibited a remarkable peak at 178 ℃ and suggested an endothermic thermal cyclization process (Figure S15). The reaction energy (ΔG = 8.09 KCal·mol^{-1}) was similar to that of *E*-CDPM (ΔG = 7.43 KCal·mol^{-1}). Thus, the comparable thermodynamic stability of these two isomers was checked and confirmed again. Likewise, a similarity in the related peak intensity of *Z*-CDPM and *E*-CDPM was also detected in the later stage of heating in the dynamic ^{1}H NMR analysis ($\geq$ 5d, Figure 2a). Together with the similar results observed in the dynamic ^{1}H NMR analysis of *E*-CDPM (Figure S16), the robustness of the thermal cyclization of *Z*/*E* CDPM was successfully validated.

Later, the photophysical properties of DPXDC were investigated. As depicted in Figure 2c-2e, the white crystal of DPXDC showed moderate blue emission, and it absorbed at 315 nm and emitted weakly at 450 nm in THF. When a poor solvent of water was added to the THF solution, not only an enhancement in the fluorescence intensity was observed due to the aggregation of DPXDC molecules, but also a gradually red-shifted emission peak was detected. This indicated that DPXDC showed both AIE property and the twisted intramolecular charge-transfer effect.[47-49] Taken together of the specific photophysical properties of DPXDC and the robustness and high efficiency of the thermal cyclization in solution, a new thermochromic motif of *Z*-CDPM thus could be coined.

Thermal elimination. Unexpectedly, when silica gel was initially added to the DCM

solution of *Z*-CDPM and then heated at 145 ℃ for 24 h to test its thermochromic behavior in the solid state, a completely different ^{1}H NMR spectrum was obtained (Figure 3a). Meanwhile, no signal of DPXDC or *Z*-CDPM was detected at all. To unlock this mystery, we purified this compound by column chromatography. A compound was isolated in 82% yield, and its molecular structure was confirmed to be DPXC by the single crystal X-ray diffraction technique (Figure 3b, Scheme S4 and Table S3). Satisfactory spectroscopical results corresponding to its molecular structure (Figure S17-S19), including the ^{1}H NMR spectrum compared with that of the final heated sample of *Z*-CDPM were also obtained (Figure 3a). In view of the appearance and gradually enhancement in intensity of these characteristic NMR peaks of DPXC at δ 8.53, 8.35-8.34, 7.87-7.84 and 7.09-7.08 in the dynamic ^{1}H NMR analysis (Figure S20), a new feasible thermal elimination process of *Z*-CDPM and the formation of DPXC in solid state was discovered. Besides, DPXC absorbed at 355 nm and emitted weakly in THF (Figure S21 and Figure 3c), and displayed an obvious enhanced emission at 460 nm in a THF/water mixture (f_w = 99%). All these suggested that it was AIE-active. Also, the white crystal of DPXC exhibited weak blue emission (Figure 3d). Considering the feasible thermochromic behavior of *Z*-CDPM in TLC plate (Figure S22), *Z*-CDPM was capable of performing functional discoloration in the solid state by the thermal elimination.

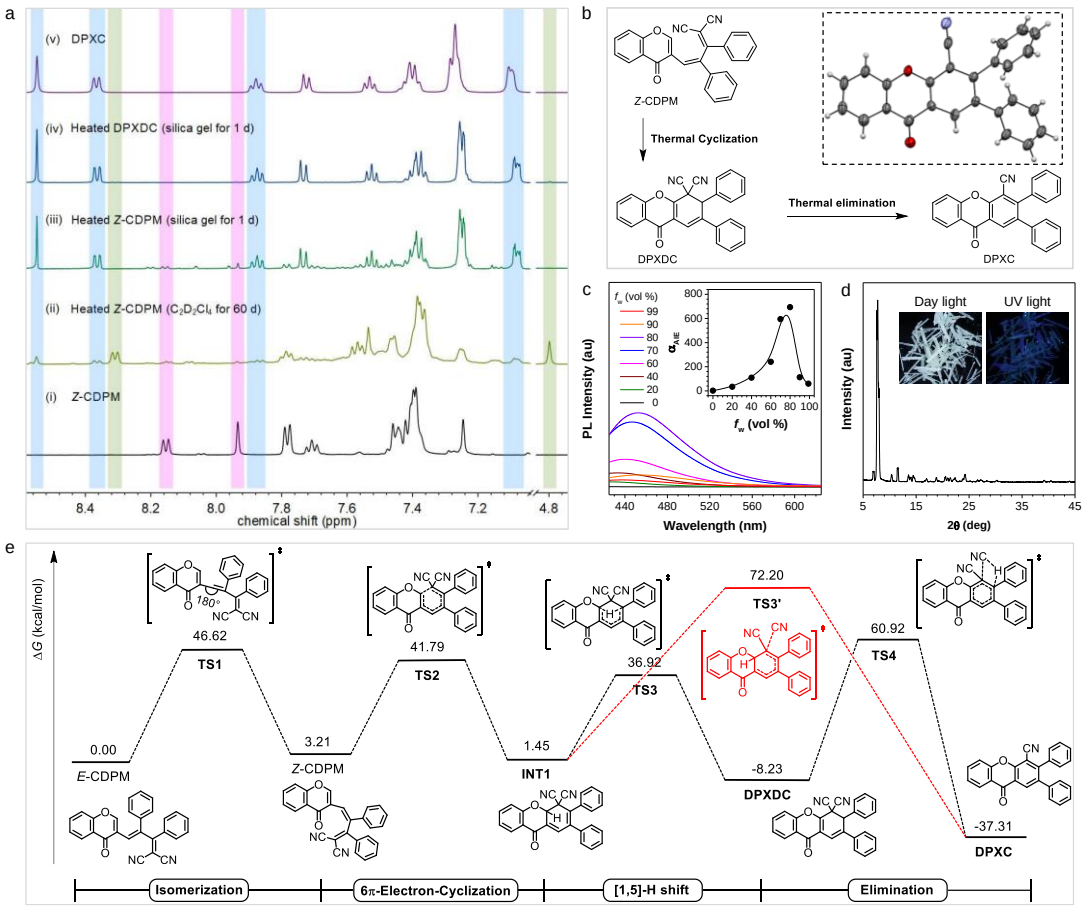

Figure 3. (a) ^{1}H NMR spectra of *Z*-CDPM before and after heating at 145 °C under different conditions. *Z*-CDPM was highlighted in purple, DPXDC was highlighted in green, and DPXC was highlighted in blue. (b) Proposed reaction routes for the formation of DPXC from Z-CDPM and DPXDC. (c) PL spectra of *Z*-DPXC (a, 10 μM) in THF/water mixtures. Inset: plots of I/I_0 value versus the f_w of THF/water mixtures of DPXC, where I_0 = PL intensity in pure THF solution. $\lambda_{ex/em}$ = 355/460 nm. (d) XRD diffractograms of the crystal powder of DPXC. Insets: photographs of crystals of DPXC. (e) Energy profile for the thermal reactions of *Z*-CDPM.

Under similar reaction conditions, DPXC was generated from DPXDC in the solid state (Figure 3a). Also, the enrichment of DPXDC after 30 days of heating appeared to accelerate the formation of DPXC in solution, which makes DPXDC a promising intermediate for the thermal elimination (Figure S23). Notably, the thermal elimination

process of *Z*-CDPM remained negligible even after 60 days of heating in solution, and meanwhile no significant changes could be found in the ^{1}H NMR spectrum of the heated crystal powder of *Z*-CDPM (Figure S24). According to the difference in molecular structure, a volatile molecule HCN should be generated in the thermal elimination. Possibly, the volatilization of HCN was effectively accelerated by dispersing *Z*-CDPM or DPXDC into silica gel, which eventually activated the thermal elimination process. Accordingly, a possible reaction pathway for the formation of DPXC was proposed and showed in Figure 3b.

Thermogravimetric analysis, on the other hand, provided important insights into the thermal stability of molecules. The thermogravimetric differential (DTG) curves of *Z*-CDPM and DPXDC were found both stable at temperature below 200 ℃, and a maximum peak at about 390 ℃ was detected for *Z*-CDPM, DPXDC and DPXC (Figure S25), illustrating their high decomposition temperature. Additionally, a small peak at around 300 ℃ appeared in *Z*-CDPM and DPXDC (Figure S25), which could be attributed to the thermal elimination process. Similar results were found in the DTG curve of *E*-CDPM as well. Therefore, the thermal elimination process of the solid powder of *Z*/*E*-CDPM and DPXDC all took place at a high temperature of around 300 ℃, and it occurred simultaneously with the thermal degradation process.

Later, density functional theory (DFT) calculation was further carried out. In the energy profile given in Figure 3e, the initial isomerization of *E*-CDPM formed a metastable product Z-CDPM (3.21 kcal/mol), which illustrated a similar thermodynamic stability as *Z*-CDPM and *E*-CDPM. As the reaction energy barrier was

as high as 46.62 kcal/mol, the isomerization was less likely to occur at room temperature. Thus, *Z*/*E*-CDPM was feasible to obtain and store. Followed, the 6π-electron-cyclization led to the formation of another metastable ring-closed intermediate called INT1 (1.45 kcal/mol), which further underwent [1,5]-H shift to give the stable thermal cyclization product DPXDC with a low energy of -8.2 kcal/mol. Considering the relative high energy barrier (38.58 and 35.47 Kcal/mol) for these two processes, it was clear that intense heating conditions were required for the thermal cyclization. Finally, elimination took place and resulted in the generation of a stable final product of DPXC (-37.31 Kcal/mol) and a by-product of HCN. Since it was necessary for INT1 to overcome a higher energy barrier of 70.75 Kcal/mol than that of DPXDC (69.15 Kcal/mol) to generate DPXC, theoretically it would get over a lower energy barrier of [1,5]-H shift (35.47 Kcal/mol) to form DPXDC. Thus, it was possible to propose a cyclization product DPXDC-mediated elimination for *Z*/*E*-CDPM. This mechanistic insight of the thermal reactions not only pointed out the reaction pathways of Z-CDPM under heating, but also provided new possibilities for molecular engineering.

Photoarrangement I. Due to the presence of the moiety of arylvinyl substituted chromone, *Z*-CDPM should undergo photoarrangement to form an isomer called HBNPMM (Figure 4a).[42,43] Curiously, we dissolved *Z*-CDPM in chloroform and then irradiated it using a 365 nm UV lamp for 2 h. As expected, the reaction product HBNPMM was isolated and well characterized (Scheme S5 and Figure S26-28). Its molecular structure was further supported by the single crystal data, indicative of the photosensitivity of *Z*-CDPM. Besides, HBNPMM absorbed at 303 nm in THF, and

exhibited AIE property in view of the gradually enhanced fluorescence at 460 nm upon water addition (Figure S29 and Figure 4b). Also, the light yellow crystal of HBNPMM (Figure S30) showed a faint blue emission, demonstrating the unique photophysical properties of HBNPMM. Upon further UV irradiation at 365 nm, the emission of *Z*-CDPM in solution was obviously blue-shifted and reached a terminal point of 460 nm after 10 s of irradiation, which was similar to that of HBNPMM (Figure 4b and 4c). Since the fluorescence intensity almost reached the plateau at the same time, a fast and traceable photoarrangement process was confirmed. Otherwise, a continuous enhancement in fluorescence intensity was observed for the weakly emissive *E*-CDPM during UV irradiation at 365 nm (Figure S31). Eventually, the photochromic behavior of *Z*/*E*-CDPM in the TLC plate under UV irradiation was demonstrated (Figure S32), confirming the capability of *Z*/*E*-CDPM in performing on-demand discoloration in real applications.

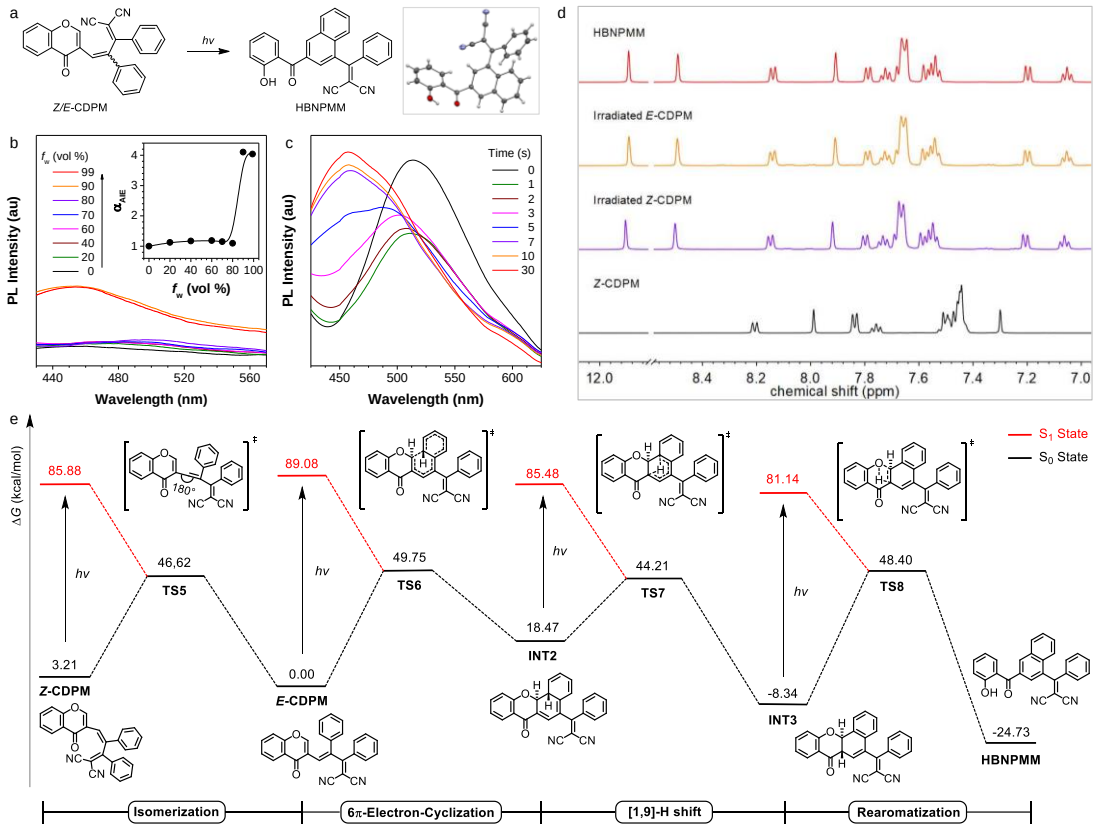

Figure 4. (a) Photoarrangement of *Z*/*E*-CDPM and single crystal structures of HBNPMM. (b) PL spectra of HBNPMM (a, 10 μM) in THF/water mixtures. λ_{ex} = 365 nm. Inset: plots of I/I_0 value versus f_w of THF/water mixtures of DPXC, where I_0 = PL intensity in pure THF solution. $\lambda_{ex/em}$ = 355/460 nm. (c) PL spectral change of *Z*-CDPM before and after UV irradiation at 365 nm for different time (1, 2, 3, 5, 7,10 and 30 s). (d) ^{1}H NMR spectra of the photoarrangement of *Z*/*E*-CDPM in $C_2D_2Cl_4$. *Z*-CDPM (red line) and *E*-CDPM (orange line) were irradiated by 365 nm UV irradiation from a 365 hand-hold UV lamp for 30 min, and the black line was HBNPMM. (e) Energy profile for the photoarrangement of *Z*-CDPM.

Considering the similarity observed in the spectral pattern of the irradiated solutions of *Z*/*E*-CDPM and HBNPMM (Figure 4d), a high-efficient photoarrangement of *Z*/*E*-CDPM and the formation of solely HBNPMM were observed. Subsequently, DFT calculations were carried out to further check the reaction pathways. As showed

from the energy profile given in Figure 4e, UV irradiation of *Z*-CDPM led to the formation of *E*-CDPM. Then, a 6π-electron-cyclization and a [1,9]-H shift process were followed to give a relatively stable intermediate (INT3) with a low energy of −8.34 kcal/mol. As previously reported, a decrease in fluorescence intensity was detected in the initial irradiation period (Figure 4c), which might be attributed to the enrichment of non-emissive metastable intermediate product INT3.[41] Afterwards, it underwent the final rearomatization to generate the stable product HBNPMM (-24.73 Kcal/mol). Since the energy barriers for these processes were high, UV irradiation was necessary to excite the molecule to overcome these energy barriers. In a word, the feasibility of arylvinyl substituted chromone as a photoactivatable motif was demonstrated.

Photoarrangement II. The limited variety of photoactivatable motifs has long puzzled scientists. Surprisingly, when a $C_2D_2Cl_4$ solution of DPXDC was irradiated under a 365 nm UV lamp, new peaks at δ 7.90-7.88, 7.65-7.62 and 6.74 were emerged and the original specific peaks of DPXDC were all disappeared 2 h later (Figure 5a). Then, we synthesized this new compound in a similar way, and a molecular structure of DPPCYM was identified according to the spectroscopical results and single crystal X-ray diffraction data (Figure S33-S35, Table S4 and Figure 5b). The similarity in the spectral pattern of the irradiated solution of DPXDC and DPPCYM (Figure 5a) further raised up the newly-discovered photorearrangement of DPXDC and the solely generation of DPPCYM under UV irradiation.

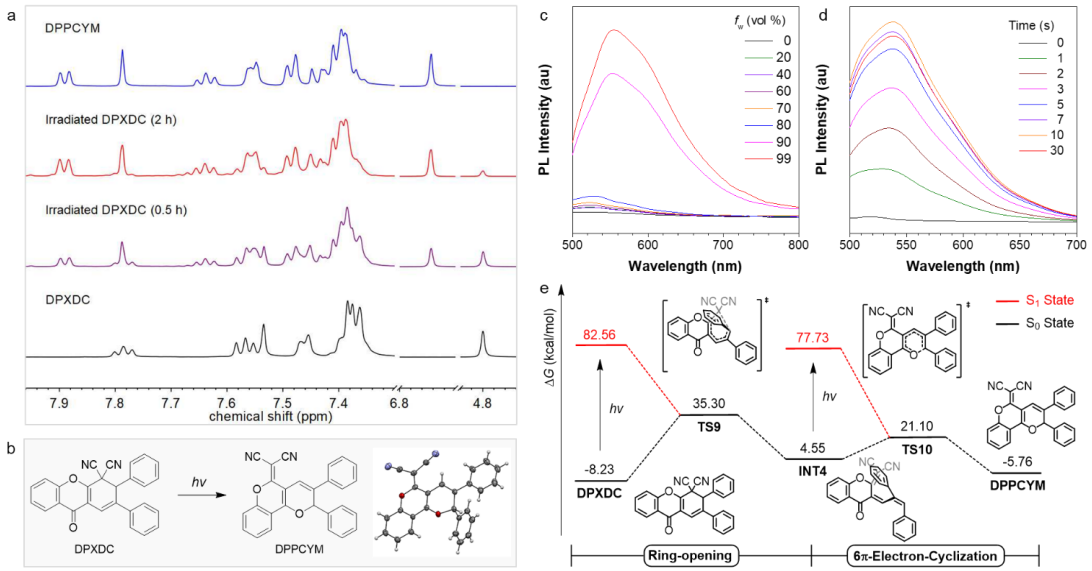

Figure 5. (a) Changes in ^{1}H NMR spectrum of DPXDC in $C_2D_2Cl_4$ during the photoarrangement process. (b) Photoarrangement of DPXDC and single crystal structure of HBNPMM. (c) PL spectra of HBNPMM (a, 10 μM) in THF/water mixtures with different water fractions (f_w). λ_{ex} = 440 nm. (d) PL spectral of DPXDC before and after UV irradiation at 365 nm for different time (1, 2, 3, 5, 7,10 and 30 s). (e) Energy profile for the photoarrangement of DPXDC.

Followed, the photophysical properties of DPPCYM and the fluorescence response of *Z*-CDPM to UV irradiation were investigated. DPPCYM displayed two main absorption peaks at 347 nm and 440 nm in THF, and its orange single crystal emitted strong yellow-green fluorescence (Figure S36 and S37). Upon water addition, an enhancement in fluorescence intensity at around 550 nm was observed, confirming the AIE property of DPPCYM. On the other hand, a gradually enhanced emission was detected for the UV irradiated sample of DPXDC in THF/water mixture with a water fraction (f_w) of 99%. Also, the fluorescence intensity almost reached a plateau after 10 s of irradiation, illustrating a fast and traceable photoarrangement process. Previously, an unexpected new peak at around 540 nm was detected for DPXDC at f_w = 99% under

365 nm excitation (Figure 3e), which might also be attributed to the generation of DPPCYM. Moreover, the photochromic behavior of DPXDC in the TLC plate was further observed(Figure S38), validating the capability of DPXDC for conducting fast and UV light-controlled coloration in the solid state.

To illustrate the reaction pathway of the newly discovered photoarrangement of DPXDC, DFT calculations were also carried out. As depicted in Figure 5e, two processes were involved in the photoarrangement of DPXDC: one was a ring-opening process with the formation of an unstable intermediate product INT4 (4.55 kcal/mol), while the another was a 6π-electron-cyclization to generate the final product DPPCYM with a low energy of -5.8 kcal/mol. For one thing, the energy barriers for these processes were high and UV irradiation was thus required to trigger their occurrence. For another thing, INT4 was not stable and the subsequent excitation energy (73.18 kcal/mol) and energy barrier (21.10 kcal/mol) was much lower than that of the former ring-opening process (90.79 kcal/mol for the excitation energy and 35.30 kcal/mol for energy barrier). Thus, INT4 will rapidly convert to DPPCYM and was not detected in the dynamic ^{1}H NMR spectra (Figure 5a). To sum up, a new photoactivatable motif of DPXDC was coined in this work and it opened new venue for molecular engineering.

Applications for information encryption. Due to the multi-responsive behaviors of *Z*-CDPM, a general strategy of constructing multifunctional systems was proposed as illustrated in Figure 6. Initially, an AIE plate of *Z*-CDPM was obtained by dip-coating a thin-layer chromatography (TLC) plate into its DCM solution and followed by air-drying process (Figure 6a). Since photochromic luminogens favor a noncontact

coloration process with high spatiotemporal resolution, a photopattern with a homemade mask of a "crab" image was then carried out to realize the "writing" process. By simply dropping the DCM solution into TLC plate and then air-drying, the different emission characteristics of these six new AIEgens on TLC plate were checked (Figure 6b). Accordingly, a blue-green-emissive "crab" image was clearly displayed in the AIE plate as expected owing to the photoconversion of *Z*-CDPM into HBNPMM in the irradiated area, while the surroundings appeared non-emissive as the initial AIE template (Figure 6c). Later, when the "fixing" process was carried out by heating the AIE plate at 200 ℃ for 30 s, strong blue emission emerged in the surrounding area of the "crab" image, attributing to the thermal elimination of *Z*-CDPM and the formation of DPXC. Before that, the thermal stability of HBNPMM and DPPCYM was also validated (Figure S39). Eventually, the "crab" was totally erased and the whole pattern became blue emissive in the "erasing" process by simply irradiating the written AIE plate. Thus, *Z*-CDPM realized *in-situ* fabricating multicolor images in a single AIEgen system.

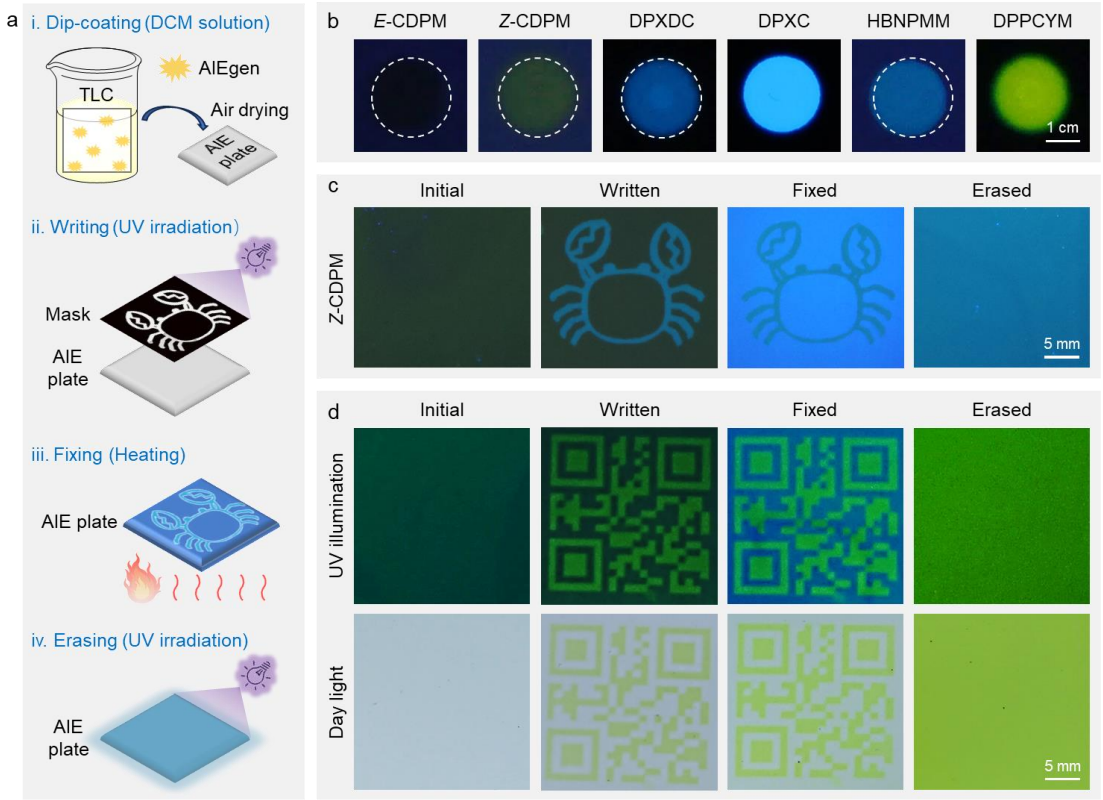

Figure 6. (a) Schematic illustration of the dip-coating of AIEgens (1 mM in DCM) on a TLC plate and the corresponding writing, fixing and erasing process through UV irradiation (10 s) or heating (200 ℃ for 10 s). b) Fluorescent images of different AIEgens on a TLC plate. Scale bar: 1 cm. c) Fluorescent images of the developed multicolor "crab" pattern of *Z*-CDPM. Scale bar: 5 mm. d) Photographs of the developed colored "QR code" of DPXDC. Scale bar: 5 mm.

Multiple coloration, on the other hand, has great potential for applications like information encryption. Since the thermal elimination and photoarrangement of *Z*-CDPM occurred at the same position of the chromone ring, it was possible to manipulate these two processes according to the sequence. Subsequently, a written quick response (QR) code was manufactured through photopatterning on an initial AIE plate. For one thing, the written QR code could be read under UV illumination, but disappeared when increasing the power of the UV light source (Figure S39). Such a

traceless and easy-operation erasure process derived from the fast photorearrangement of *Z*-CDPM was undoubtedly conducive to information security. For another thing, a colored fixed QR code with blue and blue-green fluorescence could be further obtained and it remained stable after additional UV irradiation (Figure S40 and S41). To be precise, not only a steady multicolored image could be prepared for data archiving and repeatable reading, but also the specificity of thermal elimination helped to reduce random decoding. Furthermore, the thermal elimination and photoarrangement of DPXDC occurred also at the same site of the newly-formed six-membered ring. Thus, DPXDC was applied for developing multicolored QR code as well, and similar results for information encryption were obtained (Figure 6d). To sum up, these new AIEgens (*Z*-CDPM and DPXDC) not only demonstrated their great value in the development of multifunctional systems, but also paved a specific new way to achieve high-level security information encryption system.

Conclusion

In this work, a quintuple responsive and controllable chromone-based AIEgen called *Z*-CDPM was designed and synthesized. By selecting different heating or/and irradiation conditions or tuning the aggregate morphology, this molecule exhibited efficient, quintuple and controllable thermal/photo reaction operated in the mechanisms of (i) reversible *Z*/*E* isomerization under thermal treatment; (ii) thermal cyclization in solution; (iii) thermal elimination when dispersed in silica gel; (iv) photorearrangement under UV irradiation; (v) thermal cyclization product DPXDC-mediated photorearrangement under UV irradiation. The self-reporting potential of each reaction

was also demonstrated by experimental results. In addition, single crystals were all obtained to verify these chemical structure and dynamic NMR analysis and theoretical calculations were further conducted to verify the reaction mechanisms. Based on the multiresponsiveness and controllability of *Z*-CDPM and DPXDC, multiple-colored images and a quick response code with free fixing and erasing capabilities were further manufactured for advanced information encryption. To our knowledge, *Z*-CDPM was an example of scarcity for intelligent dynamic coloration. It is anticipated that this work not only paves new ways for the design of smart luminogens with multiple responsive properties and controllability, but also provides a unique approach for constructing advanced information encryption systems based on luminescent materials.

References

1 Cuthill, I. C.; Allen, W. L.; Arbuckle, K.; Caspers, B.; Chaplin, G.; Hauber, M. E.; Hill, G. E.; Jablonski, N. G.; Jiggins, C. D.; Kelber, A.; Mappes, J.; Marshall, J.; Merrill, R.; Osorio, D.; Prum, R.; Roberts, N. W.; Roulin, A.; Rowland, H. M.; Sherratt, T. N.; Skelhorn, J.; Speed, M. P.; Stevens, M.; Stoddard, M. C.; Stuart-Fox, D.; Talas, L.; Tibbetts, E.; Caro, T. The biology of color. *Science* **2017**, *357*, eaan0221.

2 Orteu, A.; Jiggins, C.D. The genomics of coloration provides insights into adaptive evolution. *Nat. Rev. Genet.* **2020**, *21*, 461–475.

3 Cuthill, I. C.; Stevens, M.; Sheppard, J.; Maddocks, T.; Párraga, C. A.; Troscianko, T. S. Disruptive coloration and background pattern matching. *Nature* **2005**, *434*, 72–74.

4 Endler, J. A.; Mappes, J. The current and future state of animal coloration research. *Philos. Trans. R. Soc. B* **2017***, 372*, 20160352.

5 Pembury Smith, M. Q. R.; Ruxton, G. D. Camouflage in predators. *Biol. Rev. Camb. Philos. Soc.* **2020**, *95*, 1325–1340.

6 How, M. J.; Santon, M. Cuttlefish camouflage: blending in by matching background features. *Current Biology* **2022**, *32*, 523–525.

7 Sun, L.; Zhou, T.; Wan, Q. H.; Fang, S. G. Transcriptome comparison reveals key components of nuptial plumage coloration in crested ibis. *Biomolecules* **10**, 905 (2020).

8 Nam, S.; Wang, D.; Kwon, C.; Han, S. H.; Cho, S. S. Biomimetic multicolor-separating photonic skin using electrically stretchable chiral photonic elastomers. *Adv. Mater.* **2023**, *35*, 2302456.

9 Teyssier, J.; Saenko, S. V.;Marel D.;Milinkovitch, M. C. Photonic crystals cause active colour change in chameleons. *Nat. Commun.* **2015**, *6*, 6368.

10 Kim, H.; Choi, J.; Kim, K. K.; Won, P.; Hong, S.; Ko, S. H. Biomimetic chameleon soft robot with artificial crypsis and disruptive coloration skin. *Nat. Commun.* **2021**, *12*, 4658.

11 Sauvé, E. R.; Tonge, C. M.; Hudson, Z. M. Aggregation-induced energy transfer in color-tunable multiblock bottlebrush nanofibers. *J. Am. Chem. Soc.* **2019**, *141*, *41*, 16422–16431.

12 Liu, S.; Liu, X.; Yuan, J.; Bao, J. Multidimensional information encryption and storage: when the input is light. *Research* **2021**, *2021*, 7897849.

13 Liu, H.; Wei, S.; Qiu, H.; Si, M.; Lin, G.; Lei, Z.; Lu, W.; Zhou, L.; Chen, T. Supramolecular hydrogel with orthogonally responsive R/G/B fluorophores enables multi-color switchable biomimetic soft skins. *Adv. Funct. Mater.* **2022**, *32(9)*, 2108830.

14 Zhang, J., He, B., Hu, Y., Alam, P., Zhang, H., Lam, J. W. Y., Tang, B. Z. Stimuli-responsive AIEgens. *Adv. Mater.* **2021**, *33*, 2008071.

15 Zhang, X., Chen, L., Lim, K. H., Gonuguntla, S., Lim, K. W., Pranantyo, D., Yong, W. P., Yam, W. J. T., Low, Z., Teo, W. J., Nien, H. P., Loh, Q. W., Soh, S. The pathway to intelligence: using stimuli-responsive materials as building blocks for constructing smart and functional systems. *Adv. Mater.* **2019**, *31*, 1804540.

16 Zhang, H.; Li, Q.; Yang, Y.; Ji, X.; Sessler J. L. Unlocking chemically encrypted information using three types of external stimuli. *J. Am. Chem. Soc.* **2021**, *143*, 18635–18642.

17 Wang, Q.; Lin, B.; Chen, M.; Zhao, C.; Tian, H.; Qu, D. H. A dynamic assembly-induced emissive system for advanced information encryption with time-dependent security. *Nat. Commun.* **2022**, *13*, 4185.

18 Du, J.; Sheng, L.; Xu, Y.; Chen, Q.; Gu, C.; Li, M.; Zhang, S. X. Printable off-on thermoswitchable fluorescent materials for programmable thermally controlled full-color displays and multiple encryption. *Adv. Mater.* **2021**, *33*, 2008055.

19 Jiang, J.; Zhang, P.; Liu, L.; Li, Y.; Zhang, Y.; Wu, T.; Xie, H.; Zhang, C.; Cui, J.; Chen, J. Dual photochromics-contained photoswitchable multistate fluorescent

polymers for advanced optical data storage, encryption, and photowritable pattern. *Chem. Eng. J.* **2021**, *425*, 131557.

20 Huang, G.; Xia, Q.; Huang, W.; Tian, J.; He, Z.; Li, B. S.; Tang, B. Z. Multiple anti-counterfeiting guarantees from a simple tetraphenylethylene derivative–high-contrasted and multi-state mechanochromism and photochromism. *Angew. Chem. Int. Ed.* **2019**, *58*, 17814–17819.

21 Wei, P.; Zhang, J. X.; Zhao, Z.; Chen, Y.; He, X.; Chen, M.; Gong, J.; Sung, H. H.; Williams, I. D.; Lam, J. W. Y.; Tang, B. Z. Multiple yet Controllable photoswitching in a single AIEgen system. *J. Am. Chem. Soc.* **2018**, *140*, 1966−1975.

22 Zhang, Q., Yang, L., Han, Y., Wang, Z., Li, H., Sun, S., Xu, Y. A pH-sensitive ESIPT molecule with aggregation-induced emission and tunable solid-state fluorescence multicolor for anti-counterfeiting and food freshness detection. *Chem. Eng. J.* **2022**, *428*, 130986.

23 Zhu, G.; Liu, Z.; Bisoyi, H. K.; Li, Q. Controllable versatility in a single molecular system from photoisomerization to photocyclization. *Adv. Optical Mater.* **2024**, *12*, 2301908.

24 Luo, W.; Wu, B.; Xu, X.; Han, X.; Hu, J.; Wang, G. A triple pH-responsive AIEgen: synthesis, optical properties and applications. *Chem. Eng. J.* **2022**, *431*, 133717.

25 He, J.; Yang, Y.; Li, Y.; He, Z.; Chen, Y.; Wang, Z.; Zhao, H.; Jiang, G. Multiple anti-counterfeiting guarantees from simple spiropyran derivatives with solid

photochromism and mechanochromism. *Cell Reports Physical Science* **2021**, *2*, 100643.

26 Hariharan, P. S.; Mothi, E. M.; Moon, D.; Anthony, S. P. Halochromic isoquinoline with mechanochromic triphenylamine: smart fluorescent material for rewritable and self-Erasable fluorescent platform. *ACS Appl. Mater. Interfaces* **2016**, *8*, 33034–33042.

27 Zhang, J.; Shen, H.; Liu, X.; Yang, X.; Broman, S. L.; Wang, H.; Li, Q.; Lam, J. W. Y.; Zhang, H.; Cacciarini, M.; Nielsen, M. B.; Tang, B. Z. A dihydroazulene-based photofluorochromic AIE system for rewritable 4D information encryption. *Angew. Chem.Int. Ed.* **2022**, *61*, e202208460.

28 Li, X.; Li, W.; Liu, X.; Zhang, M.; Yu, E. Y.; Law, A. W. K.; Ou, X.; Zhang, J.; Sung, H. H. Y.; Tan, X.; Sun, J.; Lam, J. W. Y.; Guo, Z.; Tang, B. Z. A photoactivatable luminescent motif through ring-flipping isomerization for multiple photopatterning. *J. Am. Chem. Soc.* **2023**, *145*, 26645−26656.

29 Wang, X.; Xu, B.; Tian, W. Solid-state luminescent molecular photoswitches. *Acc. Mater. Res.* **2023**, *4*, 311−322.

30 Luo, W., Wang, G. Photo-responsive Fluorescent Materials with Aggregation-Induced Emission Characteristics. *Adv. Optical Mater.* **2020**, *8*, 2001362.

31 Zhang, J., Zou, Q. Tian, H. Photochromic materials: more than meets the eye. *Adv. Mater.* **2013**, *25*, 378–399.

32 Zhou, Q.; Qiu, X.; Su, X.; Liu, Q.; Wen, Y.; Xu, M.; Li, F. Light-responsive luminescent materials for information encryption against burst force attack. *Small* **2021**, *17*, 2100377.

33 Li, Z.; Chen, H.; Li, B.; Xie, Y.; Gong, X.; Liu, X.; Li, H.; Zhao, Y. Photoresponsive luminescent polymeric hydrogels for reversible information encryption and decryption. *Adv. Sci.* **2019**, *6*, 1901529.

34 Liang, J.; Tang, B. Z.; Liu, B. Specific light-up bioprobes based on AIEgen conjugates. *Chem. Soc. Rev.* **2015**, *44*, 2798–2811.

35 Fujita, K.; Urano, Y. Activity-based fluorescence diagnostics for cancer. *Chem. Rev.* **2024**, *124 (7)*, 4021–4078.

36 Li, H., Kim, H., Han, J., Nguyen, V., Peng, X., Yoon, J. Activity-based smart AIEgens for detection, bioimaging, and therapeutics: Recent progress and outlook. *Aggregate* **2021**, ***2***, e51.

37 He, W.; Yang, Y.; Qian, Y.; Chen, Z.; Zheng, Y.; Zhao, W.; Yan, C.; Guo, Z.; Quan, S. Fluorogenic sensing of amorphous aggregates, amyloid fibers, and chaperone activity via a near-infrared aggregation-induced emission-active probe. *Aggregate* **2023**, *4*, e412.

38 Zhou, P.; Han, K. ESIPT-based AIE luminogens: Design strategies, applications, and mechanisms. *Aggregate* **2022**, *3*, e160.

39 Wang, Y.; Li, C.; Qu, H.; Fan, C.; Zhao, P.; Tian, R.; Zhu, M. Real-time fluorescence in situ visualization of latent fingerprints exceeding level 3 details

based on aggregation-induced emission. *J. Am. Chem. Soc.* **2020**, 142(16), 7497–7505.

40 Wu, W.; Liu, B. Aggregation-induced emission: challenges and opportunities. *Natl. Sci. Rev*. **2021**, *8*, nwaa222.

41 He, X.; Xie, H.; Hu, L.; Liu, P.; Xu, C.; He, W.; Du, W.; Zhang, S.; Xing, H.; Liu, X.; Park, H.; Cheung, T. S.; Li, M.-H.; Kwok, R. T. K.; Lam, J. W. Y.; Lu, J.; Tang, B. Z. A versatile AIE fluorogen with selective reactivity to primary amines for monitoring amination, protein labeling, and mitochondrial staining. *Aggregate* **2022**, e239.

42 He, X.; Zhang, J.; Liu, X.; Jin, Z.; Lam, J. W. Y.; Tang, B. Z. A multiresponsive functional AIEgen for spatiotemporal pattern control and all-round information encryption. *Angew. Chem. Int. Ed.* **2023**, *62*, e202300353.

43 Fan, J.; Wang, T.; Li, C.; Wang, R.; Lei, X.; Liang, Y.; Zhang, Z. Synthesis of benzoaryl-5-yl(2-hydroxyphenyl)methanones via photoinduced rearrangement of (*E*)-3-arylvinyl-4H-chromen-4-ones. *Org. Lett.* **2017**, *19*, 5984–5987.

44 Liu, S.; Ou, H.; Li, Y.; Zhang, H.; Liu, J.; Lu, X.; Kwok, R. T. K.; Lam, J. W. Y.; Ding, D.; Tang, B. Z. Planar and twisted molecular dtructure leads to the high brightness of semiconducting polymer nanoparticles for NIR-IIa fluorescence imaging. *J. Am. Chem. Soc.* **2020**, *142*, *35*, 15146–15156.

45 Zhang, M.; Zhang, J.; Alam, P.; Li, W.; Lam, J. W. Y.; Jia, G.; Tang, B. Z. Hydrazone-based AIEgens with photofluorochromic ability for rewritable,

intensity-variable, and high-resolution photopattern. *Adv. Funct. Mater.* **2023**, *33*, 2213927.

46 Gonzalez, A.; Kengmana, E. S.; Fonseca, M. V.; Han, G. G. D. Solid-state photoswitching molecules: structural design for isomerization in condensed phase. *Mater. Today Chem.* **2020**, *6*, 100058.

47 Grabowski, Z. R.; Rotkiewicz, K.; Rettig, W. Structural changes accompanying intramolecular electron transfer: focus on twisted intramolecular charge-transfer states and structures. *Chem. Rev.* **2003**, *103*, *10*, 3899–4032.

48 Wang, C.; Qiao, Q.; Chi, W.; Chen, J.; Liu, W.; Tan, D.; McKechnie, S.; Lyu, D.; Jiang, X.; Zhou W.; Xu, N.; Zhang, Q.; Xu, Z.; Liu, X. Quantitative design of bright fluorophores and AIEgens by the accurate prediction of twisted intramolecular charge transfer (TICT). *Angew. Chem. Int. Ed.* **2020**, *59*, 10160–10172.

49 Wang, C.; Chi, W.; Qiao, Q.; Tan, D.; Xu, Z.; Liu, X. Twisted intramolecular charge transfer (TICT) and twists beyond TICT: from mechanisms to rational designs of bright and sensitive fluorophores. *Chem. Soc. Rev.* **2021**, *50*, 12656–12678.

50 Hu, Y.; Huang, Z.; Willner, I.; Ma, X. Multicolor circularly polarized luminescence of a single-component system revealing multiple information encryption. *CCS Chem.* **2024**, *6*, 518–527.

51 Zhang, R.; Chen, Y.; Liu, Y. Light-driven reversible multicolor supramolecular shuttle. *Angew. Chem. Int. Ed.* **2023**, *62*, e202315749.

Acknowledgements

We are grateful for financial support from the National Natural Science Foundation of China (22103062), the Research Grants Council of Hong Kong (16305320, 16307020 and C6014-20w), the Innovation and Technology Commission (ITC-CNERC14SC01), Shenzhen Key Laboratory of Functional Aggregate Materials (ZDSYS20211021111400001), and the Science Technology Innovation Commission of Shenzhen Municipality (KQTD20210811090142053 and JCYJ20220818103007014).

Author Contributions

X.H. conceived and designed the project. J.W.Y.L. and B.Z.T. supervised the work. L.H and B.H. contributed to theoretical calculation. X.H. wrote the manuscript. All coauthors analyzed the results and revised the manuscript.

Competing interests. The authors declare no competing interests.